Applied Surface Science 517 (2020) 146165

Contents lists available at ScienceDirect

Applied Surface Science

journal homepage: www.elsevier.com/locate/apsusc

Full Length Article

Temperature dependence of exchange bias in $NiFe_2O_4/BiFeO_3$ bilayers

Ji Wang[a], Chen Chen[b], Biao Xu[b], Qingyu Xu[b,*], Ruobai Liu[a], Yuan Yuan[a], Linao Huang[a], Tianyu Liu[a], Lujun Wei[a], Biao You[a], Wei Zhang[a], Jun Du[a,c,*]

[a] National Laboratory of Solid State Microstructures and Department of Physics, Nanjing University, Nanjing 210093, PR China
[b] School of Physics, Southeast University, Nanjing 211189, PR China
[c] Collaborative Innovation Center of Advanced Microstructures, Nanjing 210093, PR China

ARTICLE INFO

Keywords:
Exchange bias
Field cooling
Multiferroic material
All-oxide bilayer

ABSTRACT

In $BiFeO_3$-based ferromagnet/anitferromagnet (FM/AFM) bilayers, field cooling is required through the Néel temperature to achieve significant exchange bias (EB) at room temperature (RT). In this work, $NiFe_2O_4/BiFeO_3$ (NFO/BFO) all-oxide bilayer films were selected and deposited on $SrTiO_3$ substrates by pulsed laser deposition to avoid the possible interfacial oxidization during the field cooling process. In combination with X-ray diffraction (XRD), X-ray photoemission spectroscopy (XPS) and transmission electron microscopy (TEM) characterizations, the NFO/BFO bilayers are shown to have good crystalline layered structure. After field cooling at various temperatures, the samples show sizable EB effect at low temperature region, which is attributed to spin-glass-pinned effect. More importantly, significant EB can be obtained at RT after the sample was field cooled from temperatures higher than 400 K. The maximal values of the exchange bias field (H_E) and the ratio between H_E and coercivity (i.e. H_E/H_C) are 48 Oe and 0.6 at RT, respectively. The EB effect at RT is considered to result from the pinned and uncompensated spins near the NFO-BFO interface.

1. Introduction

Multiferroic materials simultaneously exhibit several ferroic orders, such as ferroelectricity, ferromagnetism, antiferromagnetism and so on [1]. $BiFeO_3$ (BFO) has attracted huge attention due to the coexisting ferroelectricity (FE) and antiferromagnetism, whose phase transition temperatures are both well above room temperature (RT) with ferroelectric Curie temperature (T_{CE}) of ~1100 K and antiferromagnetic (AFM) Néel temperature (T_N) of ~640 K [2,3]. Exchange bias (EB) effect, manifested itself by a shift of the magnetic hysteresis (*M-H*) loop along the magnetic axis (H_E, exchange bias field) and an enhancement of the coercivity (H_C) as well, is generally due to exchange coupling at the ferromagnetic (FM) and AFM interface [4] and has been widely used in many applications, such as read heads and magnetic sensors [5,6]. If both EB effect and magnetoelectric (ME) coupling coexist in the FM/BFO bilayer system, electric control of magnetization can be realized, which may have great potential application in next generation spintronic devices with extremely low energy consumption [2].

Although EB has been successfully realized in bilayers composed of BFO layer adjacent with many kinds of FM metallic layer, such as BFO/NiFe [7], BFO/Co [8], BFO/CoFe [9], BFO/CoFeB [10] and so on, the FM metallic layers are all deposited on AFM BFO layer in a magnetic field of hundreds of Oe and the observed EB effects are not very strong. It is well accepted that the local uncompensated spins at the BFO/FM-metal interface are responsible for the appearance of EB [9,11]. Generally, field cooling process is required through T_N of the AFM layer to establish a significant EB effect if FM layer is deposited on AFM layer. However, because BFO has relatively high T_N (~640 K) and strong chemical activity, interfacial diffusion and/or reaction between FM metallic and BFO layers will happen inevitably during field cooling [12]. On the other hand, because pure phase BFO film can only be formed at a very high temperature (~700 °C), similar problems will arise if BFO layer is deposited on FM-metal layer under an external magnetic field. In addition, BFO/FM metallic bilayer system is not ideal as there are processing incompatibilities of these two different type of materials [11]. For example, the oxidization of FM metallic layer which appears during the electrical manipulation limits the application in BFO-based devices [13].

Alternatively, an all-oxide bilayer incorporating BFO may be a good choice to replace the BFO/FM metallic combination. Recently, systematic studies have been done in BFO/$LaSrMnO_3$ [14], BFO/Fe_3O_4 [15], BFO/Sr_2FeMoO_6 [16]. Although significant EB effect can be obtained, the blocking temperature, T_B, in these bilayers are low. The effect is that the EB disappears at temperatures above T_B [17]. The low

* Corresponding authors at: National Laboratory of Solid State Microstructures and Department of Physics, Nanjing University, Nanjing 210093, PR China (J. Du).
E-mail addresses: xuqingyu@seu.edu.cn (Q. Xu), jdu@nju.edu.cn (J. Du).

https://doi.org/10.1016/j.apsusc.2020.146165
Received 19 December 2019; Received in revised form 15 March 2020; Accepted 19 March 2020
Available online 20 March 2020
0169-4332/

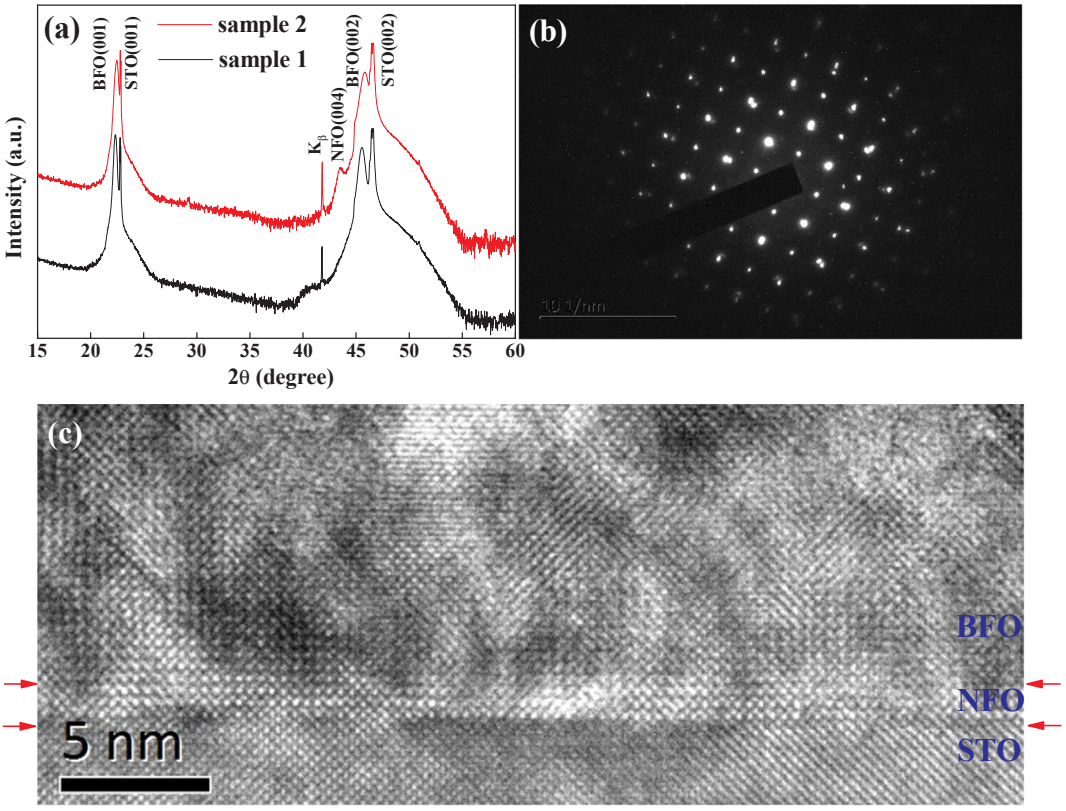

Fig. 1. (a) XRD patterns for sample 1 and sample 2. (b) The SAED pattern for sample 1. (c) The HRTEM image for sample 1. The red arrows are indications of the STO-NFO and NFO-BFO interfaces.

T_B seems uncorrelated to the high T_N of BFO and is generally ascribed to a new interface magnetic state resulted from spin reconstruction between BFO and the FM-oxide layers. For example, T_B is about 100 K in the $BiFeO_3$-$La_{0.7}Sr_{0.3}MnO_3$ (BFO-LSMO) bilayer [14], which originates from a strong hybridized interfacial magnetic state as a consequence of the electron orbital reconstruction from the LSMO and BFO $d_{3z^2-r^2}$ orbitals via oxygen 2p orbital. In the BFO/Fe_3O_4 bilayer [15], T_B is observed to be about 200 K, which is also considered to result from a novel interface state generated by the antiferromagnetic superexchange interaction between BFO and Fe_3O_4. T_B is only 160 K in the BFO/Sr_2FeMoO_6 bilayer, which is mainly ascribed to interfacial interaction of Fe-O-Fe [16].

$NiFe_2O_4$ (NFO) is a spinel ferrite and a typical soft ferrimagnetic material with high ferromagnetic Curie temperature (T_{CM}) (858 K) [18], low anisotropy and small coercivity [19]. It is promising to obtain significant EB effect with large H_E/H_C at room temperature (RT). Very recently, Wang et al. [20] reported H_E at RT in $NiFe_2O_4$/$BiFeO_3$ bilayer, which was found to be no more than 5 Oe. The H_E/H_C was found by the authors to be 4.5%. These values are low compared to ordinary FM/$BiFeO_3$ bilayers [7–10]. The much weak EB effect at RT might be due to the simple sol-gel growth method and large thickness of BFO (~215 nm) and NFO (~49 nm), resulting in rough and chemically intermixed interface with large surface roughness value (~5.88 nm) for the BFO/NFO bilayer [20]. In this work, we used pulsed laser deposition (PLD) technique to fabricate the BFO/NFO bilayer with reducing the thicknesses of BFO and NFO layers to be about 50 nm and several nanometers, respectively. With significantly improved crystallinity and interface quality, H_E and H_E/H_C at RT have been increased greatly to be about 48 Oe and 0.6, respectively. Meantime, the EB effect at temperatures below RT and its inherent mechanism have also been investigated.

2. Experimental details

The BFO ceramic target was prepared by the tartaric acid modified sol-gel method [16]. Similar method was used to prepare the NFO ceramic target. Epitaxial NFO/BFO bilayer was deposited on (0 0 1) $SrTiO_3$ (STO) substrate by PLD with a KrF excimer laser. The laser ablation was carried out with a laser fluence of 150 mJ and a repetition rate of 50 Hz. Firstly, the NFO layer was deposited on STO substrate at O_2 partial pressure of 10 Pa with the substrate temperature kept at 650 °C. Then the BFO layer was deposited subsequently on the NFO layer at O_2 partial pressure of 2 Pa with the substrate temperature kept at 700 °C. In the present studies, two representative bilayer samples were fabricated with the stacking structures as NFO (2 nm)/BFO (50 nm) (sample 1) and NFO (5 nm)/BFO (50 nm) (sample 2), respectively. For comparison, we made a control sample (i.e. sample 3) composed of a NFO single layer (2 nm) deposited on STO (0 0 1) substrate under the same conditions as those for the bilayer samples. The thicknesses labeled in parentheses are nominal values.

The X-ray diffraction (XRD) measurements were carried out by a Rigaku Smartlab3 diffractometer with Cu K_α radiation. The X-ray photoemission spectroscopy (XPS) (Thermo-scientific K-Alpha) measurements were carried out in an ultrahigh vacuum system using Al K_α radiation as the X-ray source. The transmission electron microscopy (TEM) image and selected area electron diffraction (SAED) were characterized by a JEM-2100HR equipment. The magnetic measurements were performed by a superconducting quantum interference device-vibrating sample magnetometer (SQUID-VSM, Quantum Design) with the magnetic field applied in the film plane. Before measurement the superconducting magnet has been demagnetized and the residual field is less than 5 Oe, which can be considered as the measurement error of H_E and H_C.

3. Results and discussion

Fig. 1(a) shows the XRD patterns for sample 1 and sample 2. A weak diffraction peak can be seen at $2\theta = 43.4^{\circ}$ for sample 2, corresponding to (0 0 4) crystal plane of NFO [21]. However, this peak can be hardly observed in sample 1, which may be due to a very thin NFO layer (2 nm). The obvious diffraction peaks located at $2\theta = 22.5^{\circ}$ and 45.5° correspond to (0 0 1) and (0 0 2) crystal planes of pseudocubic BFO [22], respectively. Except for the (00n) diffraction peaks of STO, no obvious impurity phases can be found. This indicates highly (0 0 1) oriented growth of NFO and BFO layers on STO substrate. In Fig. 1(b), the SAED pattern for sample 1 displays two sets of but much closed diffraction spots scattered in square shape, one of which denotes STO and the other ought to be BFO since its crystal constant is much closed to that of STO [23]. Because the NFO layer is too thin, diffraction spots are very weak and overlapped by the spots from other layers, making them difficult to be distinguished in the SAED. Fig. 1(c) provides the high-resolution TEM (HRTEM) image for sample 1, indicating that the STO-NFO interface is clear while the NFO-BFO interface is obscure. For the HRTEM investigation, if one layer is nearly epitaxially grown on the other layer, they have much similar crystalline structures, which may make the interface between them difficult to be distinguished. Similar results can be found for BFO epitaxially grown on STO substrate [24]. To confirm the quality of the NFO layer and the interface with BFO layer in sample 1, HRTEM investigation was also performed on the control sample, i.e. sample 3. As shown in Fig. S1 in Supporting Information, the NFO layer is continuous with high crystalline quality. The thickness of the NFO layer is quite uniform, implying the smooth interface with BFO layer in sample 1.

The chemical states for sample 1 were investigated by XPS depth profiling after calibrating the etching rate (~0.1 nm/s) for the BFO film. The XPS spectrum was first recorded at the sample surface and then recorded from the depth of 15 nm after the sample was etched per 5 nm in depth. Fig. 2(a)-(c) show the corresponding XPS spectra for Bi-4f, Ni-2p and Sr-3d, respectively. In Fig. 2(a), before the sample was etched, two peaks appear at the binding energies of 158.9 eV and 164.1 eV, which are corresponding to Bi^{3+}-$4f^{7/2}$ and Bi^{3+}-$4f^{5/2}$, respectively [25,26]. When the sample started to be etched, two additional peaks can be observed on the low binding energy side of Bi^{3+} peaks, which are attributed to the zero valence or metallic state of bismuth (Bi^{0}) [26]. The appearance of metallic Bi is most possibly caused by Bi–O bonding breakage and oxygen dissociation during the etching process [26]. As the sample is etched from the surface to the interior progressively, all the Bi-correlated peaks become weaker and finally vanishing when the etching depth is about 55 nm, which is approximately equal to the nominal thickness of BFO layer. In contrast to the obvious binding energy peaks of Bi^{3+}, only a very weak peak at about 854 eV could be observed in Fig. 2(b), corresponding to Ni^{2+}-$2p^{3/2}$ [27]. Moreover, this peak can only be observed at an intermediate and narrow depth range and disappears completely when the etching depth is about 50 nm, indicating a very thin $NiFe_2O_4$ layer. In Fig. 2(c), the binding energies of 133.9 eV and 135.5 eV correspond to Sr^{3+}-$3d^{5/2}$ and Sr^{3+}-$3d^{3/2}$, respectively [28]. The two peaks cannot be detected directly from the sample surface. As the etching process is underway, these two peaks begin to appear and become more obvious and approach saturation when the etching depth reaches about 60 nm. These above XPS results demonstrate a layered stacking structure of the BFO/NFO bilayer deposited on STO substrate.

One of the common methods to establish EB in FM/AFM bilayer is field cooling (FC), which means the sample is cooled from a high temperature (T_{FC}) to a low temperature with a constant magnetic field (H_{FC}) applied during the cooling process. Fig. 3 displays the *M-H* loops measured at 5 K for sample 2 (the nominal thickness of NFO is 5 nm) after it was cooled from RT (i.e. $T_{FC} = 300$ K) to 5 K under $H_{FC} = 0.5$ T and -0.5 T. The inset of Fig. 3 provides the enlarged view of the *M-H* loop ranged from -0.1 T to 0.1 T, indicating clearly that the *M-H* loop

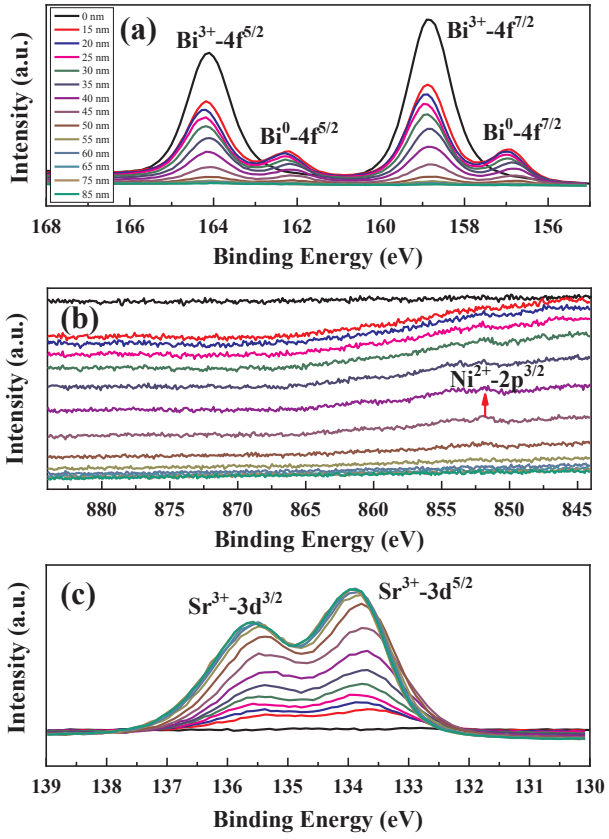

Fig. 2. The depth profile XPS spectra for (a) Bi-4f, (b) Ni-2p and (c) Sr-3d for sample 1. The red arrow in (b) is indication of the peak for Ni^{2+}-$2p^{3/2}$.

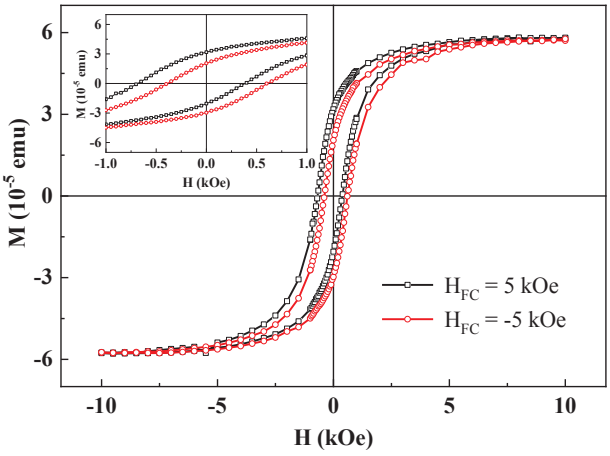

Fig. 3. The *M-H* loops measured at 5 K after sample 2 was field cooled from 300 K to 5 K under $H_{FC} = \pm 0.5$ T. The insets are the corresponding enlarge views of the *M-H* loops at low-*H* region.

shifts leftwards (rightwards) when the H_{FC} is positive (negative) and the shift amounts in both directions are almost the same. The values of H_E and H_C can be calculated by $H_E = -(H_L + H_R)/2$ and $H_C = (H_R - H_L)/2$, where H_L and H_R are the left and right coercive fields, respectively. From Fig. 3, it can be obtained that H_E and H_C are 130 Oe and 470 Oe, respectively, which unambiguously demonstrate that sizable EB can be obtained at 5 K in the NFO/BFO bilayer system through field cooling from RT to 5 K.

The temperature dependences of H_E and H_C for sample 2 with $T_{FC} = 300$ K are displayed in Figs. 4(a) and 4(b), respectively. In Fig. 4(a), with increasing *T*, H_E decreases fast initially and much slowly

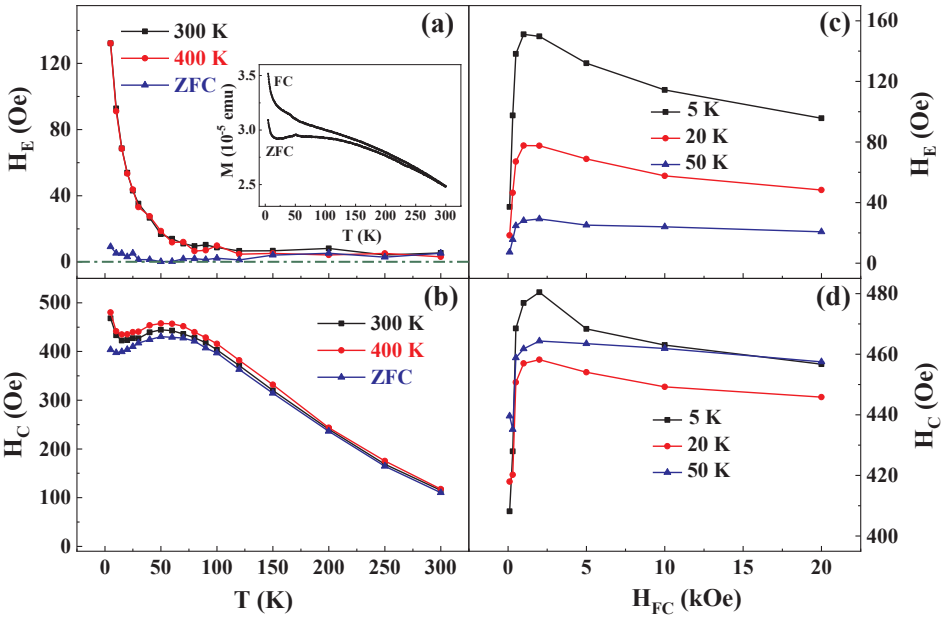

Fig. 4. (a) Temperature dependences of H_E for ZFC and FC (H_{FC} = 0.5 T, T_{FC} = 300 K and 400 K) for sample 2. The inset is the ZFC-FC *M-T* curves measured under 0.5 T for sample 2. (b) Temperature dependences of H_C for ZFC and FC (H_{FC} = 0.5 T, T_{FC} = 300 K and 400 K) for sample 2. H_{FC} dependences of H_E (c) and H_C (d) measured at T = 5 K, 20 K and 50 K for sample 2.

after T reaches about 70 K. At RT, negligible EB effect is observed with H_E less than 5 Oe, which is close to the measurement error. Fig. 4(b) exhibits that H_C decreases with increasing T generally whereas a non-monotonic variation appears at low-T region (T < 70 K). In order to know the influence of field cooling on EB, sample 2 were cooled from 300 K to 5 K under zero magnetic field (zero-field-cooling, ZFC) and the corresponding $H_E \sim T$ and $H_C \sim T$ curves are also displayed in Fig. 4(a) and 4(b), respectively. Those results show that H_E for ZFC is generally much smaller than that for FC at the same temperature in the low-T region (see in Fig. 4(a)) and H_C for ZFC is also smaller than that for FC in the entire temperature range (see in Fig. 4(b)), confirming that the EB of NFO/BFO bilayer at low temperatures is established by field cooling. Moreover, the EB studies were also performed on a 2 nm thick NFO single layer film (i.e. sample 3) after the ZFC and FC processes identical to those for sample 2. As shown in Fig. S2 in Supporting Information, H_E is negligible in the entire measuring temperature range (5 K ~ 300 K) for ZFC, while it is about 30 Oe at 5 K and decreases fast to zero with increasing T to be about 50 K for FC. These results indicate that the EB in sample 3 is much weaker than that in sample 2, confirming that the EB in the NFO/BFO bilayer mainly comes from the NFO-BFO interface at low-T region.

In order to reveal the mechanism responsible for the EB phenomena in the low-T region, ZFC-FC *M-T* curves for sample 2 were measured under H = 0.5 T, as shown in the inset of Fig. 4(a). Around T = 50 K, a peak and a kink appear at the ZFC and FC *M-T* curves, respectively, which has been attributed to the spin-glass (SG) phase transition in BFO [29]. In contrast, as shown in the inset of Fig. S2 in Supporting Information, the nearly overlapping of ZFC and FC *M-T* curves and almost continuous decrease of M with increasing T for sample 3 exclude the SG phase formation in the NFO layer. It is well known that sizable EB effect can also be observed in FM/SG bilayers, which is due to the exchange coupling between the FM and SG layers [30,31]. Due to diverse and entangled spin interactions existing in SG and the fact that these interactions can be affected by the field cooling process, the H_{FC} dependence of EB in FM/SG bilayer is quite different from that of conventional FM/AFM bilayer [32]. In FM/SG bilayers, H_E increases firstly and then decreases with increasing H_{FC} after H_{FC} exceeds the saturation field of the FM layer. Similar behavior can be also observed in the H_{FC} dependence of H_C. These results have been both experimentally and theoretically verified in FM/SG bilayers [32]. In contrast, H_E and H_C usually increase with H_{FC} in the beginning and keep almost unchanged with increasing H_{FC} further in conventional FM/AFM bilayers [33,34]. Therefore, the H_{FC} dependence of EB has been frequently used to judge whether the EB comes from SG [16,35–37]. Fig. 4(c) and (d) show the $H_E \sim H_{FC}$ and $H_C \sim H_{FC}$ curves, respectively, at T = 5 K, 20 K and 50 K for sample 2. All the curves demonstrate the similar behavior of 'increasing initially and then decreasing', agreeing well with those typical features of EB for FM/SG bilayers. Therefore, the EB in the NFO/BFO bilayer at the low-T region mainly results from the exchange coupling between NFO and SG phase in BFO.

Now we turn to discuss the EB effect at RT. When T_{FC} is increased up to 400 K, the T dependences of H_E and H_C have not changed too much in comparison with T_{FC} = 300 K, as displayed in Fig. 4(a) and (b) for sample 2. Only less than 5 Oe of H_E can be obtained for this sample at RT. In order to obtain notable EB in the NFO/BFO bilayers at RT, two approaches can be considered: (1) Reducing the thickness of NFO layer because H_E is generally inversely proportional to the thickness of FM layer in FM/AFM bilayer [17]; (2) Increasing T_{FC} to be close to or even larger than T_N of bulk BFO. Therefore, the following studies are concentrated on sample 1 (the nominal thickness of NFO is 2 nm) and T_{FC} is set as 425 K, 450 K, 475 K, 500 K, 550 K, 600 K, 650 K and 700 K, respectively. Sample 1 was field cooled from T_{FC} to RT under H_{FC} = ± 0.5 T with increasing T_{FC} successively. After each field cooling process, the *M-H* loops of the sample were measured with increasing T from 5 K to RT (i.e. 300 K) at some selected temperatures.

Fig. 5 shows four sets of *M-H* loops measured at RT with T_{FC} equal to 425 K, 550 K, 600 K and 650 K, respectively. The insets show the enlarged views of *M-H* loops at low-H region. Similar to the observation in Fig. 3, the *M-H* loop shifts leftwards (rightwards) when the H_{FC} is positive (negative), which unambiguously demonstrates that EB can be achieved at RT after field cooling with T_{FC} > 400 K for sample 1. In addition to the shift along the H axis, meantime the *M-H* loop shifts upwards (downwards) with positive (negative) H_{FC} applied. The larger the horizontal shift is, the larger vertical shift along the M axis can be observed. In principle, there is a positive (negative) shift along the M axis after the FM/AFM bilayer is field cooled with applying a positive (negative) H_{FC} when the interfacial exchange coupling is ferromagnetic [38]. Usually, the shift amount is quite small because it is produced by the interfacial pinned and uncompensated spins, whose moments are much less than those of the entire FM layer [38]. However, since the NFO layer is very thin (~2 nm) and the saturation magnetization of NFO film is quite small (~190 emu/cm^3, [39]), the vertical shift of *M-H* loops can be clearly observed. Therefore, the concurrent shifts along the H and M axes indicate that the EB effect in the NFO/BFO bilayer at RT

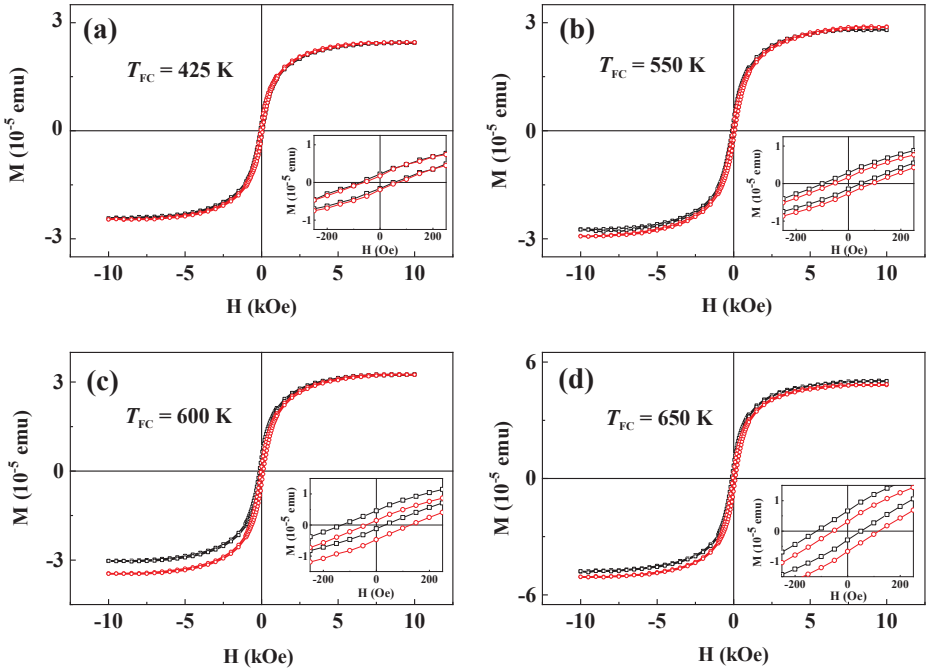

Fig. 5. *M-H* loops measured at RT for sample 1 cooled to RT under H_{FC} = 0.5 T (in black) and −0.5 T (in red) with T_{FC} equal to 425 K (a), 550 K (b), 600 K (c) and 650 K (d), respectively. The insets show the corresponding enlarged views of *M-H* loops at low-*H* region.

originates from the pinned and uncompensated spins near the NFO-BFO interface [20].

The temperature dependences of H_E and H_C for sample 1 after field cooled under H_{FC} = 0.5 T with various T_{FC} are displayed in Fig. 6. For comparison, field cooling with T_{FC} = 300 K was also performed. It can be seen that both H_E and H_C decrease monotonically with increasing T on all the curves. Each $H_E \sim T$ curve shows a sharp increase in the low-T region, which may be also due to SG-pinning as that in sample 2. However, the non-monotonic variation in low-T region is absent in all the $H_C \sim T$ curves, implying that the SG behavior in sample 1 is different from that in sample 2. The most striking result is that significant

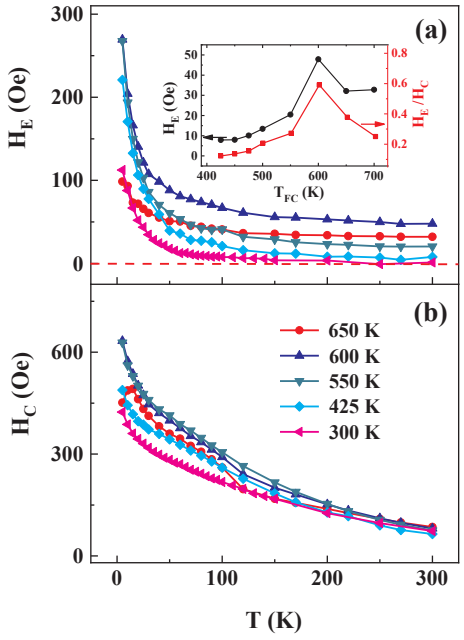

Fig. 6. Temperature dependences of H_E and H_C for sample 1 after being field cooled under H_{FC} = 0.5 T with various T_{FC}. The inset shows the T_{FC} dependences of H_E and H_E/H_C measured at RT for sample 1.

EB effect can be realized at RT with proper T_{FC}. As shown clearly in the inset of Fig. 6(a), H_E increases with T_{FC} and reaches a maximum of 48 Oe when T_{FC} is equal to 600 K, which is close to T_N of bulk BFO (~640 K) [2–3]. After that, H_E decreases with increasing T_{FC} further. The ratio of H_E/H_C is also a very important factor weighing the EB effect in application, which has the same T_{FC} dependence as that of H_E and the largest value of 0.6 when T_{FC} is equal to 600 K, as shown in the inset of Fig. 6(a). The maximal values of H_E and H_E/H_C are significantly larger than those reported before in the NFO/BFO bilayers [20] and all the other BFO-based all-oxide FM/AFM bilayers at RT. As for the gradual decrease of H_E and H_E/H_C with T_{FC} higher than 600 K, it is most possibly due to the formation of apparent BFO impurity phases (e.g. Bi_2O_3, $Bi_{25}FeO_{39}$ and etc.) generated by vacuum annealing at high temperatures, which has been verified by the XRD pattern after sample 1 was field cooled with T_{FC} = 700 K (not shown here). Therefore, 600 K is the optimized T_{FC} in the present NFO/BFO bilayer systems. For comparison, the 2 nm thick NFO single film (i.e. sample 3) was also field cooled from 600 K to RT under 0.5 T. The *M-H* loop measured at RT is displayed in Fig. S3 in Supporting Information. From this it can be obtained that H_E and H_C are 1.4 Oe and 34.4 Oe, respectively, which are much smaller than those (48 Oe/80 Oe) for sample 1 after field cooling from 600 K. Therefore, it can be concluded that the EB effect obtained at RT after field cooling with T_{FC} larger than 400 K for the NFO/BFO bilayer also comes from the NFO-BFO interface, similar to that at low-T region.

4. Conclusions

In summary, NFO/BFO bilayer films were deposited on STO substrates by pulsed laser deposition technique. High-quality crystallinity with highly (0 0 1) oriented growth and layered structure of the NFO/BFO bilayers were confirmed by XRD, TEM and XPS. After being field cooled from various T_{FC}, significant EB effect can be observed at low temperatures and RT as well. A sharp increase of H_E at low-T region is attributed to the exchange coupling between the NFO layer and the SG phase in BFO, determined by the cooling field dependence of EB. However, the EB effect obtained at RT is resulted from the pinned and uncompensated spins at the NFO-BFO interface. Most importantly, H_E and H_E/H_C can be achieved respectively to be 48 Oe and 0.6 at RT when

T_{FC} equals 600 K. These striking results suggest that the NFO/BFO bilayer may be a good candidate for making electric-field-control spintronic devices in the future.

CRediT authorship contribution statement

Ji Wang: Investigation, Methodology, Formal analysis, Writing - original draft. **Chen Chen:** Investigation, Methodology. **Biao Xu:** Investigation, Methodology. **Qingyu Xu:** Conceptualization, Methodology, Writing - review & editing. **Ruobai Liu:** Investigation. **Yuan Yuan:** Investigation. **Linao Huang:** Investigation. **Tianyu Liu:** Investigation. **Lujun Wei:** Methodology, Investigation. **Biao You:** Methodology, Resources. **Wei Zhang:** Resources. **Jun Du:** Conceptualization, Supervision, Writing - original draft, Writing - review & editing.

Declaration of Competing Interest

The authors declare that they have no known competing financial interests or personal relationships that could have appeared to influence the work reported in this paper.

Acknowledgements

This work was supported by National Key Research and Development Program of China (2016YFA0300803), National Natural Science Foundations of China (Nos. 51971109, 51771053, 51471085).

Appendix A. Supplementary material

Supplementary data to this article can be found online at https://doi.org/10.1016/j.apsusc.2020.146165.

References

[1] N. Spaldin, M. Fiebig, The renaissance of magnetoelectric multiferroics, Sci. 309 (2005) 391–392.
[2] M. Bibes, A. Barthélémy, Towards a magnetoelectric memory, Nat. Mater. 7 (2008) 425–426.
[3] D. Lebeugle, D. Colson, A. Forget, M. Viret, P. Bonville, J.F. Marucco, S. Fusil, Room-temperature coexistence of large electric polarization and magnetic order in $BiFeO_3$ single crystals, Phys. Rev. B 76 (2007) 024116.
[4] W.H. Meiklejohn, C.P. Bean, New magnetic anisotropy, Phys. Rev. 102 (1956) 1413–1414.
[5] J. Nogués, I.K. Schuller, Exchange bias, J. Magn. Magn. Mater. 192 (1999) 203–232.
[6] C. Chappert, A. Fert, F.N. Van Dau, The emergence of spin electronics in data storage, Nat. Mater. 6 (2007) 813–823.
[7] J. Dho, M.G. Blamire, Controlling the exchange bias in multiferroic $BiFeO_3$ and NiFe bilayers, J. Appl. Phys. 106 (2009) 073914.
[8] H. Naganuma, M. Oogane, Y. Ando, Exchange biases of Co, Py, $Co_{40}Fe_{40}B_{20}$, $Co_{75}Fe_{25}$, and $Co_{50}Fe_{50}$ on epitaxial $BiFeO_3$ films prepared by chemical solution deposition, J. Appl. Phys. 109 (2011) 07D736.
[9] L.W. Martin, Y.H. Chu, M.B. Holcomb, M. Huijben, P. Yu, S.J. Han, D. Lee, S.X. Wang, R. Ramesh, Nanoscale control of exchange bias with $BiFeO_3$ thin films, Nano Lett. 8 (2008) 2050.
[10] D. Lebeugle, A. Mougin, M. Viret, D. Colson, J. Allibe, H. Béa, E. Jacquet, C. Deranlot, M. Bibes, A. Barthélémy, Exchange coupling with the multiferroic compound $BiFeO_3$ in antiferromagnetic multidomain films and single-domain crystals, Phys. Rev. B 81 (2010) 134411.
[11] E.M. Choi, E. Weal, Z.X. Bi, H.Y. Wang, A. Kursumovic, T. Fix, M.G. Blamire, J.L. MacManus-Driscoll, Strong room temperature exchange bias in self-assembled $BiFeO_3$-Fe_3O_4 nanocomposite heteroepitaxial films, Appl. Phys. Lett. 102 (2013) 012905.
[12] T. Yu, H. Naganuma, W.X. Wang, Y. Ando, X.F. Han, Annealing temperature dependence of exchange bias in $BiFeO_3$/CoFe bilayers, J. Appl. Phys. 111 (2012) 07D908.
[13] Q.Y. Xu, Z.Y. Xu, M.C. He, Y.Q. Cao, J. Du, Irreversible electrical manipulation of magnetization on $BiFeO_3$-based heterostructures, J. Appl. Phys. 117 (2015) 17D707.
[14] P. Yu, J.-S. Lee, S. Okamoto, M.D. Rossel, M. Huijben, C.-H. Yang, Q. He, J.X. Zhang, S.Y. Yang, M.J. Lee, Q.M. Ramasse, R. Erni, Y.-H. Chu, C.-C. Kao, L.W. Marin, R. Ramesh, Interface ferromagnetism and orbital reconstruction in $BiFeO_3$-$La_{0.7}Sr_{0.3}MnO_3$ heterostructures, Phys. Rev. Lett. 105 (2010) 027201.
[15] T.L. Qu, Y.G. Zhao, P. Yu, H.C. Zhao, S. Zhang, L.F. Yang, Exchange bias effects in epitaxial Fe_3O_4/$BiFeO_3$ heterostructures, Appl. Phys. Lett. 100 (2012) 242410.
[16] C. Chen, L. Guo, C. Li, B.Z. Gao, R.K. Zheng, J. Wang, Q. Li, J. Du, Q.Y. Xu, Exchange bias in tetragonal-like $BiFeO_3$/Sr_2FeMoO_6 bilayer, J. Magn. Magn. Mater. 464 (2018) 156–160.
[17] A.E. Berkowitz, K. Takano, Exchange anisotropy - a review, J. Magn. Magn. Mater. 200 (1999) 552–570.
[18] S.M. Yusuf, P.K. Manna, M.M. Shirolkar, S.K. Kulkami, R. Tewari, G.K. Dey, A study of exchange bias in $BiFeO_3$ core/$NiFe_2O_4$ shell nanoparticles, J. Appl. Phys. 113 (2013) 173906.
[19] T.Y. Kim, S. Song, H.M. Jang, J.A. Peters, Y.K. Jeong, Piezoelectrically enhanced exchange bias in multiferroic heterostructures, J. Mater. Chem. C. 2 (2014) 8018–8022.
[20] C.H. Wang, L. Zhou, Q.Y. Fu, Y.H. Tian, S. Wang, H.B. Gou, J.B. Ai, L. Zhang, F. Xue, Exchange bias in spin-glass-like $NiFe_2O_4$/$BiFeO_3$ heterojunction at room temperature, J. Magn. Magn. Mater. 449 (2018) 372–377.
[21] Y.M. Xia, Z.M. He, Y.L. Lu, B. Tang, S.P. Sun, J.B. Su, X.P. Li, Fabrication and photocatalytic property of magnetic $SrTiO_3$/$NiFe_2O_4$ heterojunction nanocomposites, RSC Adv. 8 (2018) 5441–5450.
[22] Q.Y. Xu, Y. Sheng, X.B. Xue, X.Y. Yuan, Z. Wen, J. Du, Exchange bias in $BiFeO_3$/$La_{0.67}Sr_{0.33}MnO_3$ bilayers, Jpn. J. Appl. Phys. 53 (2014) 08NM01.
[23] Q.Y. Xu, Y. Sheng, M. Khalid, Y.Q. Cao, Y.T. Wang, X.B. Qiu, W. Zhang, M.C. He, S.B. Wang, S.Q. Zhou, Q. Li, D. Wu, Y. Zhai, W.Q. Liu, P. Wang, Y.B. Xu, J. Du, Magnetic interactions in $BiFe_{0.5}Mn_{0.5}O_3$ films and $BiFeO_3$/$BiMnO_3$ superlattices, Sci. Rep. 5 (2015) 9093.
[24] C.L. Chen, S.H. Lv, J.J. Li, Z.C. Wang, X.B. Liang, Y.X. Li, D. Viehland, K. Nakajima, Y.C. Ikuhara, Two-dimensional electron gas at the Ti-diffused $BiFeO_3$/$SrTiO_3$ interface, Appl. Phys. Lett. 107 (2015) 031601.
[25] D. Singh, T. Tabari, M. Ebadi, M. Trochowski, M.B. Yagci, W. Macyk, Efficient synthesis of $BiFeO_3$ by the microwave-assisted sol-gel method: "A" site influence on the photoelectrochemical activity of perovskites, Appl. Surf. Sci. 471 (2019) 1017–1027.
[26] Z.H. Zhang, X.L. Zhong, H. Liao, F. Wang, J.B. Wang, Y.C. Zhou, Composition depth profiles of $Bi_{3.15}Nd_{0.85}Ti_3O_{12}$ thin films studied by X-ray photoelectron spectroscopy, Appl. Surf. Sci. 257 (2011) 7461–7465.
[27] L.J. Wei, Z.Z. Hu, G.X. Du, Y. Yuan, J. Wang, H.Q. Tu, B. You, S.M. Zhou, J.T. Qu, H.W. Liu, R.K. Zheng, Y. Hu, J. Du, Full electric control of exchange bias at room temperature by resistive switching, Adv. Mater. 30 (2018) 1801885.
[28] C. Vamala, S. Manandhar, J. Kelber, Pt interactions with annealed and chemically-etched Nb-doped $SrTiO_3$(001) surfaces: Metal/oxide surface chemical effects on band bending behavior, Surf. Sci. 603 (2009) 33–39.
[29] S.N. Dong, Y.P. Yao, Y. Hou, Y.K. Liu, Y. Tang, X.G. Li, Dynamic properties of spin cluster glass and the exchange bias effect in $BiFeO_3$ nanocrystals, Nanotechnology 22 (2011) 385701.
[30] M. Ali, P. Adie, C.H. Marrows, D. Greig, B.J. Hickey, R.L. Stamps, Exchange bias using a spin glass, Nat. Mater. 6 (2007) 70–75.
[31] F.T. Yuan, J.K. Lin, Y.D. Yao, S.F. Lee, Exchange bias in spin glass (FeAu)/NiFe thin films, Appl. Phys. Lett. 96 (2010) 162502.
[32] W.B. Rui, Y. Hu, A. Du, B. You, M.W. Xiao, W. Zhang, S.M. Zhou, J. Du, Cooling field and temperature dependent exchange bias in spin glass/ferromagnet bilayers, Sci. Rep. 5 (2015) 13640.
[33] I.L. Guhr, O. Hellwig, C. Brombacher, M. Albrecht, Observation of perpendicular exchange bias in [Pd/Co]-CoO nanostructures: Dependence on size, cooling field, and training, Phys. Rev. B 76 (2007) 064434.
[34] J. Keller, P. Miltényi, B. Beschoten, G. Güntherodt, Domain state model for exchange bias. II. Experiments, Phys. Rev. B 66 (2002) 014431.
[35] M. Fan, W.R. Zhang, J. Jian, J.J. Huang, H.Y. Wang, Strong perpendicular exchange bias in epitaxial $La_{0.7}Sr_{0.3}MnO_3$: $LaFeO_3$ nanocomposite thin films, APL Mater. 4 (2016) 076105.
[36] S. Zhou, J. Wang, Y.K. Weng, Z.T. Wu, Z.H. Ni, Q.Y. Xu, J. Du, S. Dong, Synthesis, optical and magnetic properties of $Ba_2Ni_3F_{10}$ nanowires, ACS Appl. Mater. Interfaces 8 (2016) 26213–26219.
[37] M. Khan, A. Albagami, Cooling field dependent exchange bias in $Mn_2Ni_{1.4}Ga_{0.6}$: A reentrant spin glass system with short range ferromagnetic ordering, J. Alloys Compd. 727 (2017) 100–106.
[38] D.Z. Yang, J. Du, L. Sun, X.S. Wu, X.X. Zhang, S.M. Zhou, Positive exchange biasing in GdFe/NiCoO bilayers with antiferromagnetic coupling, Phys. Rev. B 71 (2005) 144417.
[39] S. Venzke, R.B. van Dover, J.M. Phillips, E.M. Gyorgy, T. Siegrist, C.-H. Chen, D. Werder, R.M. Fleming, R.J. Felder, E. Coleman, R. Opila, Epitaxial growth and magnetic behavior of $NiFe_2O_4$ thin films, J. Mater. Res. 11 (1996) 1187–1198.